Modeling viscosity of CO_2 at high temperature and pressure conditions

Menad Nait Amar [a], Mohammed Abdelfetah Ghriga [b,c], Hocine Ouaer [d], Mohamed El Amine Ben Seghier [e,f,***], Binh Thai Pham [g,**], Pål Østebø Andersen [h,*]

[a] *Département Etudes Thermodynamiques, Division Laboratoires, Sonatrach, Boumerdes, Algeria*
[b] *Institut des Sciences Analytiques et de Physico-chimie pour l'Environnement et les Matériaux, IPREM, UMR 5254, CNRS Université de Pau et des Pays de l'Adour/E2S, 2 avenue P. Angot, Technopôle Hélioparc, 64000, Pau, France*
[c] *Laboratoire Génie Physique des Hydrocarbures, Faculté des Hydrocarbures et de la Chimie, Université M'Hamed Bougara de Boumerdes, Avenue de l'Indépendance, 35000, Boumerdes, Algeria*
[d] *Département Gisement Miniers et Pétroliers, Université M'hamed Bougara de Boumerdes, Algeria*
[e] *Division of Computational Mathematics and Engineering, Institute for Computational Science, Ton Duc Thang University, Ho Chi Minh City, Viet Nam*
[f] *Faculty of Civil Engineering, Ton Duc Thang University, Ho Chi Minh City, Viet Nam*
[g] *Institute of Research and Development, Duy Tan University, Da Nang, 550000, Viet Nam*
[h] *Department of Energy Resources, University of Stavanger, 4036, Norway*

ARTICLE INFO

ABSTRACT

The present work aims at applying Machine Learning approaches to predict CO_2 viscosity at different thermo-dynamical conditions. Various data-driven techniques including multilayer perceptron (MLP), gene expression programming (GEP) and group method of data handling (GMDH) were implemented using 1124 experimental points covering temperature from 220 to 673 K and pressure from 0.1 to 7960 MPa. Viscosity was modelled as function of temperature and density measured at the stated conditions. Four backpropagation-based techniques were considered in the MLP training phase; Levenberg-Marquardt (LM), bayesian regularization (BR), scaled conjugate gradient (SCG) and resilient backpropagation (RB). MLP-LM was the most fit of the proposed models with an overall root mean square error (RMSE) of 0.0012 mPa s and coefficient of determination (R^2) of 0.9999. A comparison showed that our MLP-LM model outperformed the best preexisting Machine Learning CO_2 viscosity models, and that our GEP correlation was superior to preexisting explicit correlations.

1. Introduction

Carbone dioxide (CO_2) is the main contributor to greenhouse gas (GHG) emissions with up to 72% of the total GHG emissions recorded in 2010. Its effects on the climate and environment has become a great concern for both industry and academia (Norhasyima and Mahlia, 2018; Gambhir et al., 2017). Major efforts have been undertaken in the last decade to reduce CO_2 emissions, especially from industrial processes. Two key strategies have been developed and adopted; carbon capture and storage (CCS) and carbon capture and utilization (CCU) (Cuéllar-Franca and Azapagic, 2015). As per CCS, the CO_2 is stored in underground geological formations including saline aquifers, depleted oil/gas reservoirs, and other geological options (Aminu et al., 2017). Storage in deep ocean water (Khatiwala et al., 2013; Adams and Caldeira, 2008) and CO_2 mineral carbonation (Gerdemann et al., 2007; Oelkers et al., 2008) are also considered good alternatives for underground storage. However, the most promising alternative nowadays is to reuse captured CO_2 for other industrial purposes (Abas and Khan, 2014). CO_2 is widely used in enhanced oil and gas recovery (EOR and EGR) (Gong and Gu, 2015; Al-Bayati et al., 2018; Yu et al., 2015; Pu et al., 2016) and enhanced coalbed methane recovery (ECBM) (Mazzotti et al., 2009; Liu et al., 2019). Developments of the last decade have also indicated that CO_2 injection can be a viable option for enhanced oil and gas recovery in tight shale reservoirs (Yu et al., 2014; Sheng, 2015; Eshkalak et al., 2014; Hoffman and others, 2012; Jin et al., 2017). In particular, studies (Nuttal, 2010; Busch et al., 2008; Klewiah et al., 2020) have

* Corresponding author.
** Corresponding author.
*** Corresponding author.
E-mail addresses: m.naitamar@univ-boumerdes.dz (M.N. Amar), ghriga.ma@univ-pau.fr (M.A. Ghriga), ouaerhocine@univ-boumerdes.dz (H. Ouaer), benseghier@tdtu.edu.vn (M. El Amine Ben Seghier), phamthaibinh2@duytan.edu.vn (B.T. Pham), pal.andersen@uis.no (P.Ø. Andersen).

demonstrated that CO_2 has greater adsorption affinity than methane in shales and can both be stored effectively and lead to more efficient shale gas production. Alternative industrial applications include the use of CO_2 as a refrigerant in heating and refrigerating processes (Sawalha et al., 2017; Li et al., 2016), as feedstock in the production of chemicals (Ampelli et al., 2015; Chen et al., 2016) and carbon source for micro-algae to produce biofuels (Taher et al., 2015; Aslam et al., 2018).

Designing and optimizing the above processes requires a thorough understanding of the thermo-physical properties of CO_2 which include PVT relations, enthalpy, thermal conductivity, viscosity, and diffusion coefficient to name some (Islam and Carlson, 2012). More precisely, the viscosity of CO_2 is one of the most crucial parameters for successful implementation and forecasting of numerous applications. In CO_2-EOR projects, the viscosity of CO_2 is in a direct relationship with its mobility inside the reservoir (Eshraghi et al., 2016). For CO_2 flooding, low volumetric sweep efficiencies were always associated with the high viscosity contrast between CO_2 and other reservoir fluids (Yu et al., 2015). Likewise, the viscosity determines indirectly the energy and cost efficiency of CO_2 transportation by pipeline (Zhang et al., 2006), as is the case for CCS projects in USA and Canada (Cole and Itani, 2013). In fact, the viscosity is indirectly related through the Reynolds number with the pressure drop during flow in pipelines, which in turn affects the power consumption of pumps and compressors. It was reported that a viscosity underestimation of 30%, will lead to a 30% underestimation of the pump/compressor power consumption (Li et al., 2011).

Great attention was paid historically to study the viscosity of CO_2 experimentally and theoretically by developing models and correlations able to predict its variation at different fluid states, mixtures, and operating conditions. The available experimental data on the viscosity of CO_2 were thoroughly reviewed and compiled by Li et al. (2011) and more recently by Laesecke and Muzney (Laesecke and Muzny, 2017). As for the theoretical part, the CO_2 viscosity can be calculated using equations of state (EoS) or models based on EoS (Fan and Wang, 2006; Guo et al., 1997). Particularly, the Span and Wagner EoS (Span and Wagner, 1996) was dedicated for CO_2 property predictions. Empirical correlations were also developed. One of the first predictive correlations was reported by Chung et al. (1988). Their generalized correlation allowed the estimation of viscosity of polar, nonpolar, and associating pure fluids (including CO_2) and mixtures over a wide range of fluid states. However, this method was shown to be consistent with measurements only in the case of low-pressurized gases. Fenghour et al. (1998) improved a prior correlation established by Vesovic et al. (1990) which had suffered some deficiencies in the liquid region due to inconsistencies in some of the considered experimental data they employed when developing their model. The new correlation covered a wider range of temperatures (200–1500K) and pressures (from 0.1 up to 300 MPa). To date, the most complete correlation was established recently in 2017 by Laesecke and Muzney (Laesecke and Muzny, 2017). The authors employed all available viscosity data to develop this correlation in conjunction with the Span and Wagner EoS. The final correlation covered temperatures from 100 to 2000 K for gaseous CO_2 and from 220 to 700 K for compressed and supercritical liquid states. Considering the work by Laesecke and Myzney to be the state of the art, we will later compare our results to their correlation.

With the emergence of artificial intelligence, the trend in this research area now consists of using heuristic algorithms in modeling and predicting CO_2 properties based on the large existing set of experimental data. Zhang et al. (2018) used general regression neural network (GRNN) and back-propagation neural network (BPNN) algorithms in the prediction of CO_2 solubility, solution density and viscosity in potassium lysintae (which has a primary amine group such as monoethanolamine (MEA) solution due to a carbon-nitrogen bond (Kumar et al., 2003)) with various operating conditions and liquid concentrations. Besides, the structure–property relationships between ionic liquids, with different molecular structures, and their CO_2 solubilities were investigated by Venkatraman et al. (Venkatraman and Alsberg, 2017) using

random forests (RF), conditional inference trees (CTREE), and partial least squares regression (PLSR); and by Ouaer et al. (2020) by applying machine learning algorithms such as multilayer perceptron (MLP) and gene expression programming. Recently, Abdolbaghi et al. (2019) reported the application of four computer-based models namely particle swarm optimization (PSO), multilayer perceptron (MLP), hybrid-adaptive neuro fuzzy inference system (hybrid-ANFIS) and coupled simulated annealing-least square support vector machine (CSA-LSSVM) in the prediction of CO_2 viscosity at high temperatures and pressures. Many studies have shown high ability of machine learning algorithms to offer faster and more robust computational schemes than the classical empirical correlations and methods and can thus save time and costs related to designing or performing future experimental studies (Javadian et al., 2018; Hemmati-Sarapardeh et al., 2013; Nait Amar et al., 2019a; Ayegba et al., 2017; Ahmadi et al., 2018; Raja et al., 2017; Shokir et al., 2017; Benamara et al., 2019a).

The main purpose of this study is to advance the research on development of high exactness and simple-to-use machine learning approaches that can predict the viscosity of CO_2. This will be done by modeling CO_2 viscosity as function of temperature and density based on an extensive database encompassing wide ranges of pressure and temperature conditions. To do so, three advanced data-driven techniques, namely multilayer perceptron (MLP), group method of data handling (GMDH) and gene expression programming (GEP) were implemented. Both the GMDH and GEP methods produce the output as an explicit function of the input parameters, where GMDH applies a polynomial form while for GEP the type of mathematical operations is user specified. Numerous statistical and graphical assessment criteria were considered in the evaluation of the newly proposed models. A comparison of the performance of our results with the best available prior Machine Learning models and with well performing explicit correlations was performed. A trend analysis was conducted to observe variations of CO_2 viscosity with respect to density and temperature. Further, outlier detection was performed to quantify potential experimental points deviating from main trends in the database.

There are some important differences between this work and existing studies where ML has been applied to model CO_2 viscosity: (1) more widespread temperature (220–673 K) and pressure (0.1–7960 MPa) range conditions were considered in the training of the models, (2) four backpropagation based learning algorithms were evaluated in the training of the MLP based CO_2 viscosity model, (3) this study is not limited to black box ML models, but also two distinct explicit correlations for CO_2 viscosity based on GMDH or GEP were derived, (4) The database of experimental points and the best of the developed ML models are provided in Excel files to the benefit of the readers.

The rest of the paper follows this structure: Section 2 describes the database and main assumptions utilized in this study to develop the models and explicit correlations. Section 3 summarizes the implemented data-driven techniques. Results are presented and discussed in Section 5. The study is summarized in Section 6.

2. Data gathering and preparation

Consistent models need to be developed from a reliable database that contains a large number of experimental measurements. The viscosity of CO_2 has been investigated experimentally in several studies, where the effects of variables such as temperature and pressure on this parameter were in focus. Among such works, Laesecke and Muzney (Laesecke and Muzny, 2017) gathered the largest known database on CO_2 viscosity as function of temperature and pressure.

In this work, a widespread experimental database including 1124 samples for CO_2 viscosity with corresponding values of temperature, density and pressure was utilized for developing the proposed models. These experimental measurements were collected from several literature sources (Laesecke and Muzny, 2017; Van Der Gulik, 1997; Haepp, 1976; Vogel and Barkow, 1986; Golub'ev, 1970; Estrada-Alexanders and

Hurly, 2008; Abramson, 2009; Kestin and Whitelaw, 1963; Vogel, 2016; Michels et al., 1957; Schäfer et al., 2015; Hendl et al., 1993).
The database was randomly divided into a training set (80% of the database) and a test set (20% of the database). Table 1 represents the ranges of variables applied in this study. Our models (either using MLP, GMDH or GEP) assumed that the viscosity of CO_2 could be modelled as function of temperature and density, in line with the literature (Laesecke and Muzny, 2017; Abdolbaghi et al., 2019) where it has been claimed that more accuracy can be obtained using density rather than pressure as the second input parameter. Hence, the models and correlations take the following form:

$$\mu_{CO_2} = f(T, \rho) \tag{1}$$

When performing the modeling task using MLP, the data points were normalized between −1 and 1:

$$x_{norm} = \frac{2(x_i - x_{min})}{(x_{max} - x_{min})} - 1 \tag{2}$$

where x_{norm} is the normalized value of x_i, x_{min} and x_{max} are the minimum and maximum values of the variable x (corresponding to viscosity, temperature and density), respectively. The data were not normalized when applying the GMDH or GEP methods. Mean square error (MSE) was considered as the assessment function during the training phase of the different models. MSE is defined as follows:

$$MSE = \frac{1}{N} \sum_{i=1}^{N} (\mu_i^{exp} - \mu_i^{pre})^2 \tag{3}$$

where μ is the viscosity of CO_2, N is the number of samples in the dataset and the superscript *exp* and *pre* indicate experimental and predicted values, respectively.

3. Modeling techniques

3.1. Multilayer perceptron (MLP)

Artificial neural network (ANN) is one of the most robust data-driven methods. This approach is characterized with a high ability to recognize and identify relationships between input and output parameters in complex systems (Hemmati-Sarapardeh et al., 2018a). The learning strategy and the manner of processing information in ANN were inspired by the human brain (Hemmati-Sarapardeh et al., 2018b). Multilayer perceptron (MLP) is one of the most frequently utilized types of ANN for modeling purposes (Nait Amar et al., 2019a, 2019b) and is the first Machine Learning approach we apply here.

The MLP model consists mainly of two principal elements: neurons and layers. The neurons are considered the basic component of any ANN. In the case of MLP, the neurons are distributed beneath 3 different kinds of layers, namely the input, hidden and output layers. The input layer is where the inputs (density and temperature data in this case, i.e. two neurons) are given to the model. The output layer is where the output (CO_2 viscosity, i.e. one neuron) are returned. For a given neuron j in layer i (not in the input layer), the input x_{ij} consists of a linearly weighted sum of the outputs from the neurons of the previous layer y_{i-1j} plus a bias term b_{ij}. The output y_{ij} of the given neuron is the evaluation of this input by an activation function f_i (which can vary from layer to layer):

$$x_{ij} = b_{ij} + \sum_{j}^{N_{i-1}} w_{i-1,j} y_{i-1,j} \quad (j = 1 : N_j) \tag{4}$$

$$y_{ij} = f_i(x_{ij}) \tag{5}$$

An MLP model contains at least one hidden layer. Generally, one hidden layer allows to identify the relationships in simple to moderately complex systems, while more than one hidden layer is mandatory in highly complex systems (Haykin, 2001). Indeed, the role of hidden layers is to map the inputs into higher features by means of activation functions. These latter are generally of a non-linear type such as Logsig and Tansig:

$$\text{Logsig: } g(x) = \frac{1}{e^x + 1} \tag{6}$$

$$\text{Tansig: } g(x) = \frac{e^x - e^{-x}}{e^x + e^{-x}} \tag{7}$$

Pureline is generally the proper transfer function for the output layer.

$$\text{Pureline: } f(x) = x \tag{8}$$

A trial and error method is frequently considered when looking for the best number of hidden layers, their numbers of neurons as well as the proper activation and transfer functions.

3.1.1. Training

The training phase of the MLP model aims to find appropriate values for the weights and bias terms in order to minimize the gap between the predictions and the real values. Back-propagation (BP) learning approaches are suitable for this purpose and we applied four such alternatives to train the MLP method: Levenberg-Marquardt (LM) algorithm, bayesian regularization (BR), scaled conjugate gradient (SCG), and resilient backpropagation (RB). For more information about these algorithms, the readers are referred to some previous works (Hemmati-Sarapardeh et al., 2018b; Nait Amar et al., 2019b; Benamara et al., 2019b; Nait Amar and Zeraibi, 2019). The four resulting models are denoted MLP-LM, MLP-BR, MLP-SCG and MLP-RB.

3.2. Group method of data handling (GMDH)

Group Method of Data Handling (GMDH) is another neural network method which provides the output as an explicit mathematical correlation of the input parameters (Dargahi-Zarandi et al., 2017). It is also called polynomial neural network (PNN) as its structure consists of nodes organized in one or more intermediate layers and its generated expression is given in a polynomial form such as the quadratic form, introduced to GMDH by Ivakhnenko (1971). The relation between inputs $x_i, x_j, …, x_k$ to a node and the output Y from the node is expressed as follows:

$$Y = a + \sum_{i=1}^{D} b_i x_i + \sum_{i=1}^{D} \sum_{j=1}^{D} c_{ij} x_i x_j + \sum_{i=1}^{D} \sum_{j=1}^{D} … \sum_{k=1}^{D} d_{ij…k} x_i x_j x_k \tag{9}$$

a, b_i, c_{ij} and $d_{ij…k}$ are the coefficients of the polynomial and D is the number of inputs to the node. In this work, two nodes were applied, each as a third degree polynomial function of two input parameters (with $D = 2$ and terms up to third order in Eq. (9)). The first nodes output was a polynomial function of the inputs density and temperature, while the node 2 output (giving viscosity) was a polynomial function of density and the output from node 1. Generally, the number of nodes and order of the polynomial can be tuned. The coefficients of the polynomials (as in Eq. (9)) were optimized by applying the least square errors method formulated as:

Table 1
Ranges of the parameters in the gathered database used for the model development.

Variables	Temperature (K)	Pressure (MPa)	Density (kg/m^3)	Viscosity (mPa s)
Minimum	220	0.1	0.208	0.011189
Maximum	685.07	7960	2126.4	4.836

$$\min \sum_{i=1}^{N} \left(y_i^{GMDH} - y_i \right)^2 \qquad (10)$$

In this equation, y_i is the experimental value of viscosity, y_i^{GMDH} the value suggested by the polynomial formula and N is the number of training samples. To achieve the final trained GMDH model, the problem in Eq. (10) is resolved first by a transformation of y into matrix form (Dargahi-Zarandi et al., 2017; Hemmati-Sarapardeh and Mohagheghian, 2017):

$$y = A^T X \qquad (11)$$

and the solution is then given as:

$$A^T = y X^T \left(X X^T \right)^{-1} \qquad (12)$$

where X is the matrix composed of vectors of input products for each data point appearing in the combined polynomial term and A is the corresponding vector of coefficients. In the present work we note that hybrid GMDH was employed which allows (1) interactions between nodes from different layers and (2) the combination of more than two independent variables at a time. These two advantages raise more flexibility when dealing with complicated modeling cases (Rostami et al., 2019). The final correlation gained from the hybrid version of GMDH is presented below:

$$Y_i = a + \sum_{i=1}^{D} \sum_{j=1}^{D} \dots \sum_{k=1}^{D} \theta_{ij\dots k} x_i^n x_j^n \dots x_k^n \quad n = 1, 2, \dots, 2^L \qquad (13)$$

where $\theta_{ij\dots k}$ mean the coefficients of the polynomial and L is the number of layers.
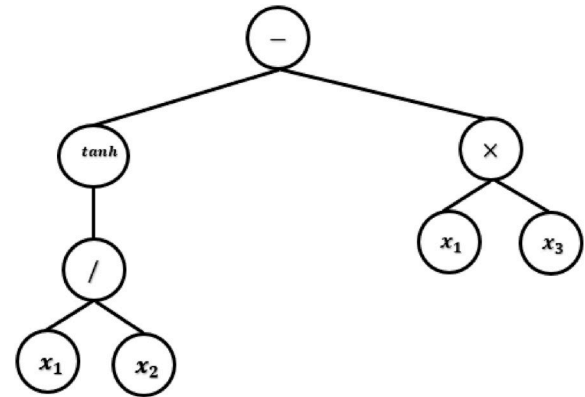
3.3. Gene expression programming (GEP)

Gene expression programming (GEP) is, similar to GMDH, a data-driven technique generating explicit (mathematical) expressions. It was proposed by Ferreira (2001) as an ameliorated version of the so-called genetic programming (GP) introduced by Koza (1992). GEP is regarded as an evolutionary technique, and hence, for the searching process to find the most fit explicit correlation, it applies the fundamental genetic operators (e.g. selection, crossover, mutation) and some other specific demarches that did not exist in the earliest version of evolutionary algorithms.

The GEP search process begins with creating a set of possible solutions (termed 'chromosomes'). In this case, the possible solutions represent different explicit correlations. The chromosomes are made up of 'genes' which are fixed length terms involving variables (such as $\{x_1, x_2, x_3\}$) and operators (such as $\{+, /, \times, -, tanh, ln\}$) (Teodorescu and Sherwood, 2008). Fig. 1 illustrates a scheme of a chromosome including two genes and its converted expression. The main steps performed in GEP for reaching the accurate correlation are given as follows:

- Setting the GEP control parameters: population size (the number of chromosomes/correlations in each generation), the number of genes (i.e. the maximum numbers of terms, also called the length), the

Fig. 1. A scheme of a chromosome with two genes (length of 2) and its expression.

- Each solution is optimized to fit the data by determining the involved coefficients using the Least Square approach.
- Each chromosome in the population is evaluated based on a fitness function indicating its performance. In our case, mean square error (MSE) was used.
- The next generation of solutions is generated using:
  - Elitism: the most fit element in the current population is saved for the following generation.
  - Selection and recombination: individuals are picked which will be recombined to give new offspring.
  - Mutation: modify elements within a genome according to a mutation rate.
  - Transposition, inversion and insertion of sequences: this is done by adding or inverting parts of the genome in the chromosome to improve the prediction ability of the correlations (Ferreira, 2001).
- The new population is then evaluated and the calculation steps from elitism operators are repeated until a stopping criterion is satisfied.

4. Results and discussion

In the MLP approach, trial and error was considered for selecting the proper number of layers and nodes and the control parameters of the various employed learning algorithms. The best-found structure in the four proposed MLP paradigms was three hidden layers covering 11, 11 and 9 neurons, respectively. Tansig was the optimal activation function in all the hidden layers, while Pureline was the optimal transfer function for the output layer. The main control parameters applied in the GEP algorithm are stated in Table 2. Two nodes with third order polynomials were applied in GMDH.

The obtained correlations after using GMDH and GEP techniques are expressed as follows:

- GMDH

$$\mu_{CO_2} = \big[-18.88275518 + 87.5583665 \times N_1 - 0.0201583 \times \rho + 0.06274136 \times \rho \times N_1 - 132.1632815 \times N_1^2 - 7.75167912 \times 10^{-6} \times \rho^2$$

$$-0.048814178 \times \rho \times N_1^2 + 1.22248704 \times 10^{-5} \times \rho^2 \times N_1 + 67.216781 \times N_1^3 - 1.02923375 \times 10^{-9} \times \rho^3 \big]^{10}$$

considered operators and the mutation rate.
- Create an initial population of chromosomes (possible correlation form).

where T and ρ are temperature and density, respectively, and the node N_1 is given below:

Table 2
GEP setting parameters used in the study.

Parameters	Value/setting
Chromosome	250
Gene	8
Mutation rate	0.4
Inversion rate	0.08
Operators	EXP, TANH, +, −, ×,/, X^2, INV, Ln, $\sqrt{}$.

$$N_1 = 0.59588907 + 0.00016937 \times \rho + 0.00022378 \times T - 2.48160084$$
$$\times 10^{-7} \times T \times \rho + 2.87964698 \times 10^{-8} \times \rho^2 - 7.69580232 \times 10^{-8} \times T^2$$
$$- 9.93679405 \times 10^{-11} \times T \times \rho^2 + 2.427651934 \times 10^{-10} \times T^2 \times \rho$$
$$+ 4.234529146 \times 10^{-11} \times \rho^3 - 1.883695528 \times 10^{-11} \times T^3$$

$$(15)$$

● GEP

$$\mu_{CO_2} = \left[0.5703 + 0.01033\sqrt{T - 11.69} - 0.0001304 \right.$$
$$\left. \times A + 0.134 \times B + 10^{-5} \times \left(\sqrt{\rho}\right) \times C \right]^{10} \quad (16)$$

In this equation, T and ρ are temperature and density, respectively, and A, B and C are defined as shown below:

$$A = \rho + T + \ln(\rho) \quad (17)$$

$$B = \tanh\left(\frac{T}{\rho}\right) - 0.271194 \times \tanh\left(\frac{\rho}{T}\right) - 0.063664 \times \tanh(T - \rho) \quad (18)$$

$$C = 1.624 \times (T + \rho) - 2.363 \times \sqrt{T \times \rho} - 480.8 \quad (19)$$

In the above explicit correlations (14) to (19), T and ρ should be given in units of K and kg/m^3 respectively to obtain viscosity μ_{CO_2} in
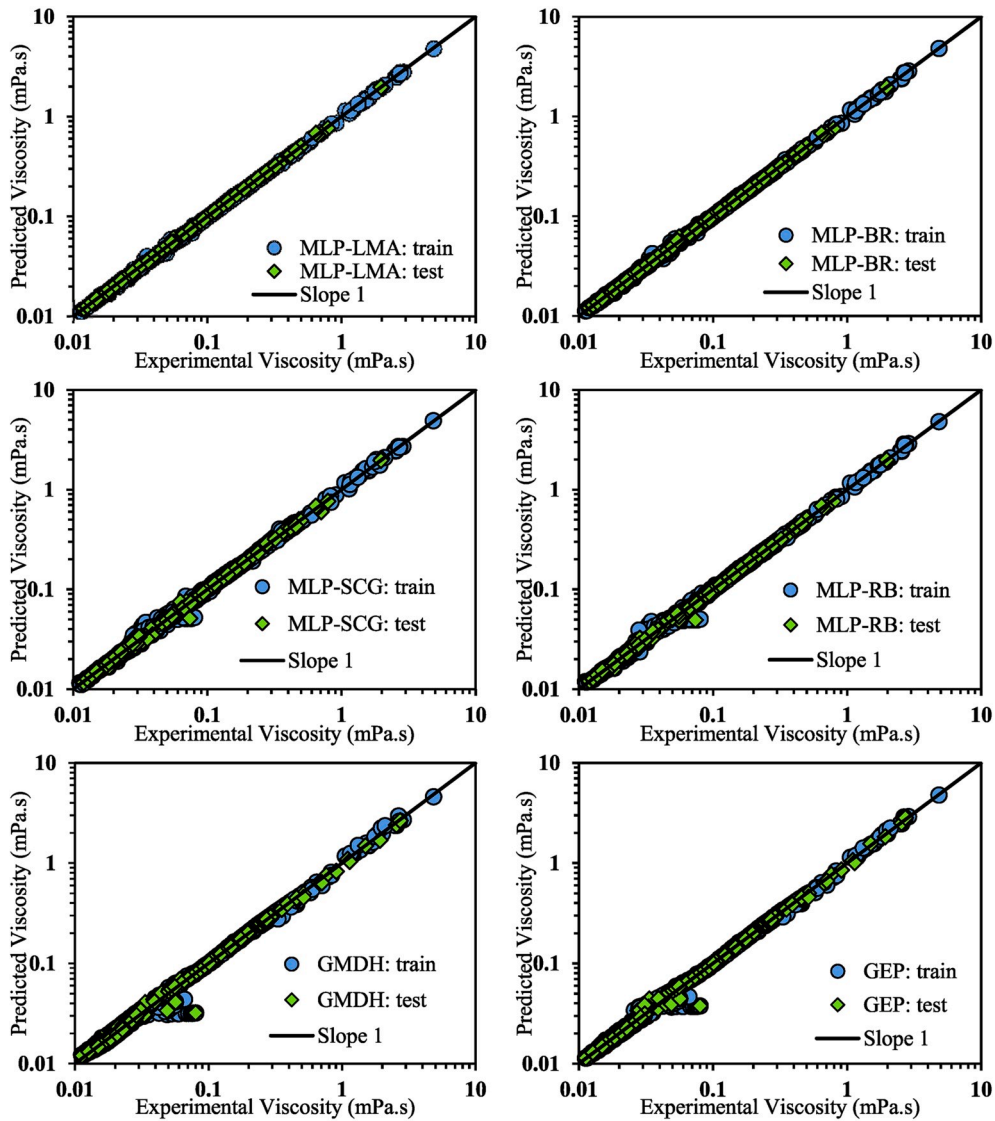

Fig. 2. Cross plots of the proposed predictive models.

units of mPa s.

4.1. Performance evaluation

To evaluate the performance and robustness of the proposed models, statistical indicators, namely root mean square error (RMSE) and coefficient of determination (R^2) are used in the evaluation. The mathematical expressions of the latter are specified as follows:

$$RMSE = \sqrt{\frac{1}{N} \sum_{i=1}^{N} \left(\mu_i^{exp} - \mu_i^{pred} \right)^2} \tag{20}$$

$$R^2 = 1 - \frac{\sum_{i=1}^{N} \left(\mu_i^{exp} - \mu_i^{pred} \right)^2}{\sum_{i=1}^{N} \left(\mu_i^{exp} - \overline{\mu_i^{pred}} \right)^2} \tag{21}$$

Fig. 2 illustrates the obtained cross plots for the different models showing predicted CO_2 viscosity versus the experimental data. The reference unit slope corresponds to perfect match. It is seen that all the models exhibit very satisfactory distributions of predictions near the unit slope line for both training and testing datasets, demonstrating high reliability in estimating the viscosity of CO_2. By close inspection, the MLP-LM and MLP-BR models have the least scatter around the unit slope line, while more scatter is seen for the MLP-SCG and MLP-RB and even more for GMDH and GEP models. The goodness of the match is illustrated more directly in Fig. 3 which shows comparative bar plots of RMSE and R^2 values for the proposed models evaluated on the overall dataset. As seen, all models have R^2 values almost identical to 1, indicating very good prediction, although the RMSE values clearly distinguish between the models in terms of their matching ability. Especially, these values demonstrate the same quality trend as seen visually in Fig. 2. The statistical parameters of the calibrated models evaluated for the training, test and overall datasets are listed in Table 3. Evaluation of
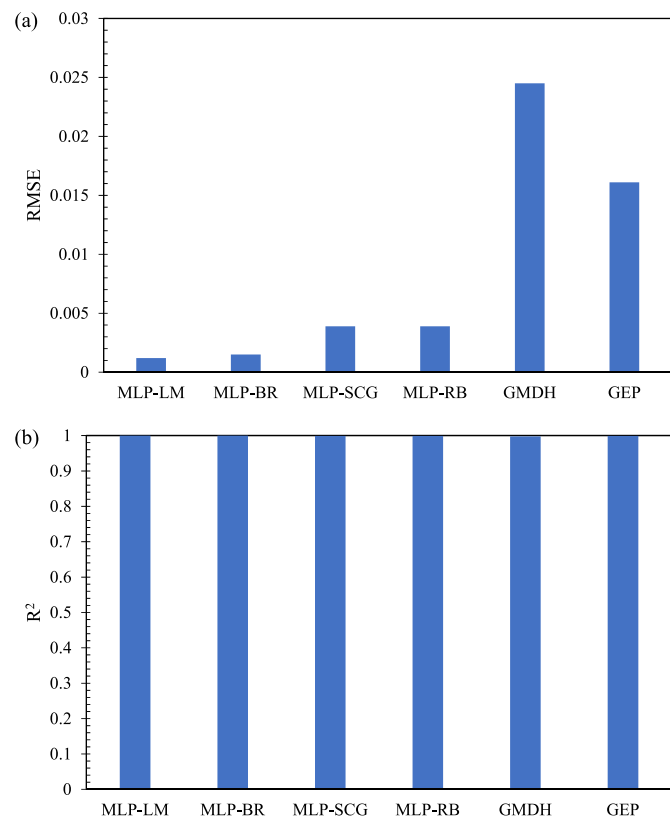
Table 3
Statistical parameters for the developed models for prediction of CO_2 viscosity as evaluated on the indicated datasets.

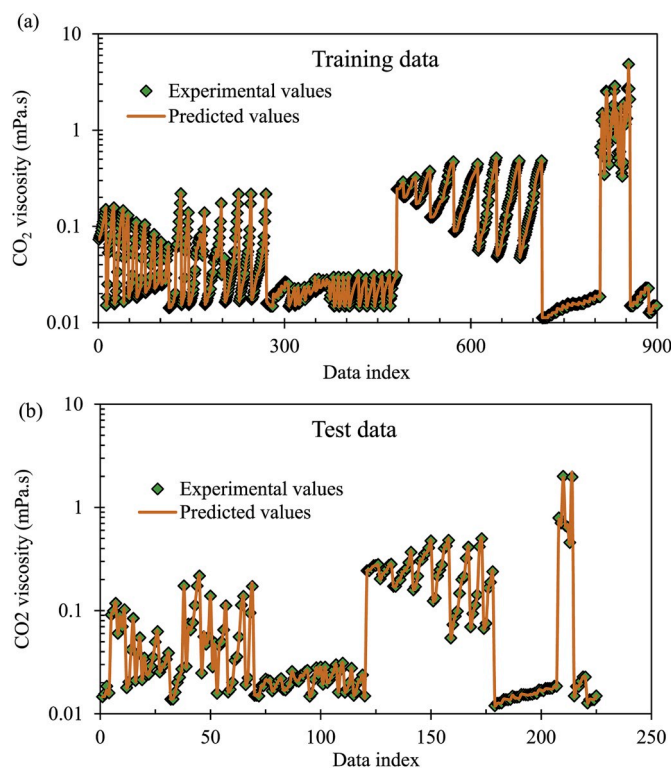|	Training data		Test data		Overall	
	RMSE	R^2	RMSE	R^2	RMSE	R^2
MLP-LM	0.0012	0.9999	0.0011	0.9999	0.0012	0.9999
MLP-BR	0.0015	0.9999	0.0013	0.9999	0.0015	0.9999
MLP-SCG	0.0041	0.9992	0.0033	0.9994	0.0039	0.9992
MLP-RB	0.0042	0.9992	0.0029	0.9995	0.0039	0.9992
GMDH	0.0251	0.9974	0.0221	0.9990	0.0245	0.9977
GEP	0.0156	0.9991	0.0180	0.9995	0.0161	0.9992

Fig. 4. Measured vs. predicted CO_2 viscosity (MLP-LM): (a) training data; (b) test data.

the statistical parameters reported in Table 3 and Fig. 3, shows that the MLP model optimized using LM is the most accurate model. It has the highest coefficient of determination during training, testing and overall ($R^2 = 0.9999$ in each), and lowest RMSE values, namely 0.0012, 0.0011 and 0.0012, respectively. It can also be noticed from Table 3 and Fig. 3 that the reliability of the developed models takes the following order: MLP-LM > MLP-BR > MLP-SCG > MLP-RB > GEP > GMDH. Furthermore, regarding the models providing explicit correlations, the GEP-based correlation outperforms that obtained with GMDH. Accordingly, the MLP-LM model will be considered for further evaluations and comparison with prior machine learning models from the literature, and the GEP-based correlation is compared with existing explicit correlations from the literature for predicting the viscosity of CO_2.

Fig. 4 shows a comparison between the MLP-LM predicted CO_2 viscosity values and the experimental values for training and test sets. This figure reveals that the majority of the predictions during the training and testing phases are in line with the measurements. Fig. 5 presents the relative error distribution of the MLP-ML model in a contour map plotted against temperature and density. Very small relative errors are achieved.
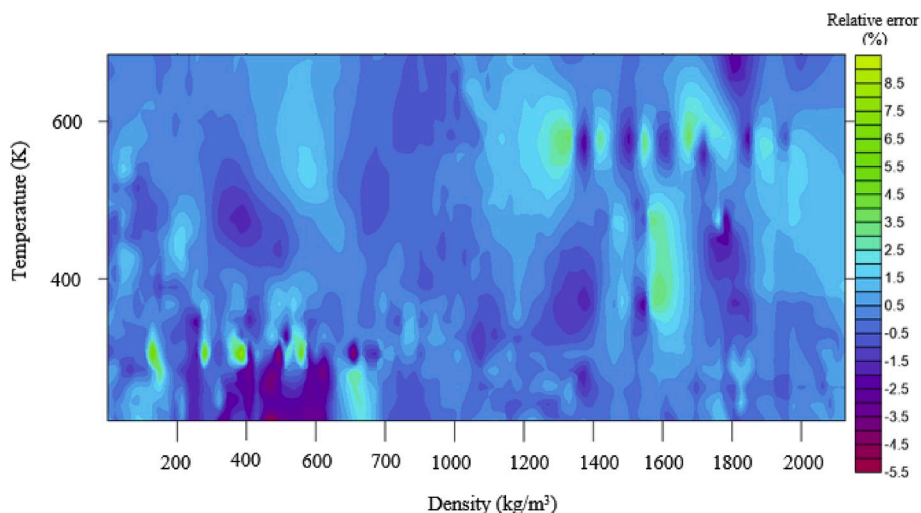

Fig. 3. Performances comparison of the proposed smart models: (a) RMSE, and (b) R^2.

Fig. 5. Relative error distribution with respect to density and temperature.

Table 4
Comparison of performance with prior models.

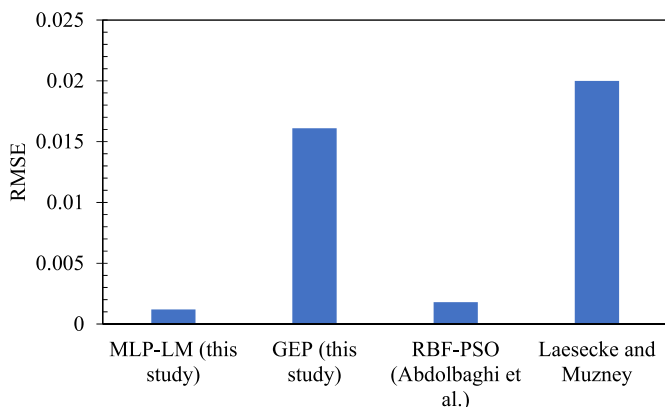|	RMSE
MLP-LM (this study)	0.0012
GEP (this study)	0.0161
RBF-PSO (Abdolbaghi et al.)	0.0018
Laesecke and Muzney correlation	0.020

Fig. 6. RMSE comparison of our best models with the best models known from the literature. RMSE was evaluated using the entire experimental dataset.

4.2. Comparison with the existing models

To compare performance of the proposed MLP-LM model and the GEP model correlation in estimation of CO_2 viscosity, two prior approaches were selected; the best established paradigm by Abdolbaghi et al. (2019), which consists of a radial basis function neural network optimized by PSO (RBF-PSO) and the correlation of Laesecke and Muzney (Laesecke and Muzny, 2017). The four stated models were applied to the collected CO_2 viscosity database. The performance results of the models by Abdolbaghi et al. (2019) and Laesecke and Muzney (Laesecke and Muzny, 2017) are stated and compared with our newly proposed models (MLP-LM and GEP) in Table 4 and Fig. 6. As demonstrated, our best implemented smart model (MLP-LM) outperforms the best prior model proposed by Abdolbaghi et al. (2019), with an RMSE of 0.0012 compared to 0.0018. In addition, the newly developed explicit correlation using GEP shows better match for predicting the viscosity of CO_2 compared to that of Laesecke and Muzney (Laesecke and Muzny,
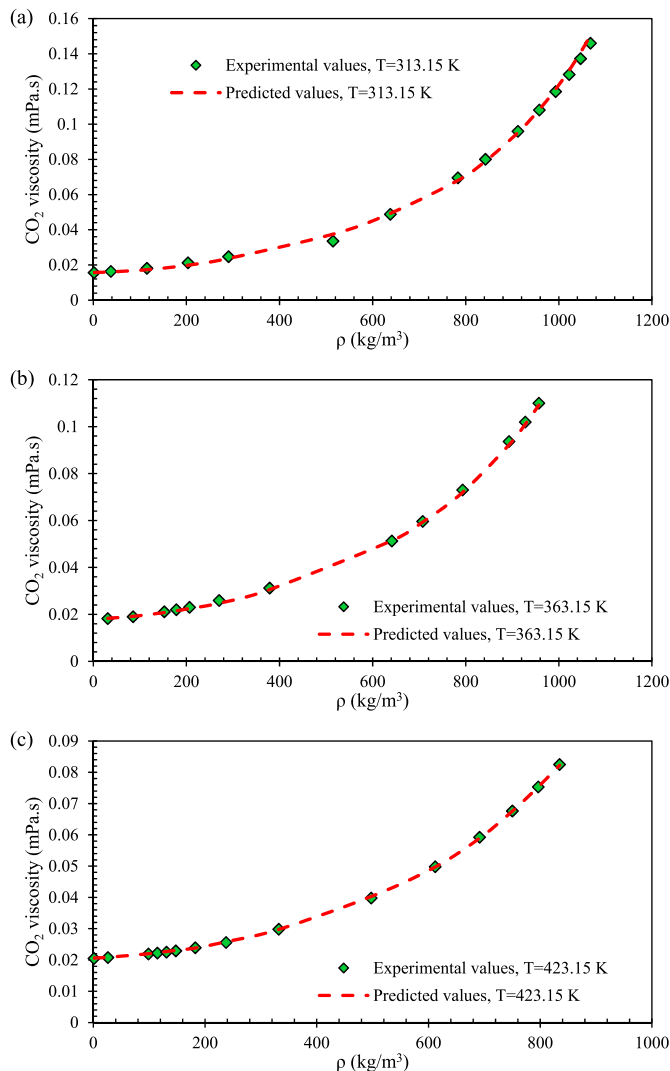

Fig. 7. Variation of CO_2 viscosity with respect to density for fixed temperatures. The predicted values are obtained by the calibrated MLP-LM model.
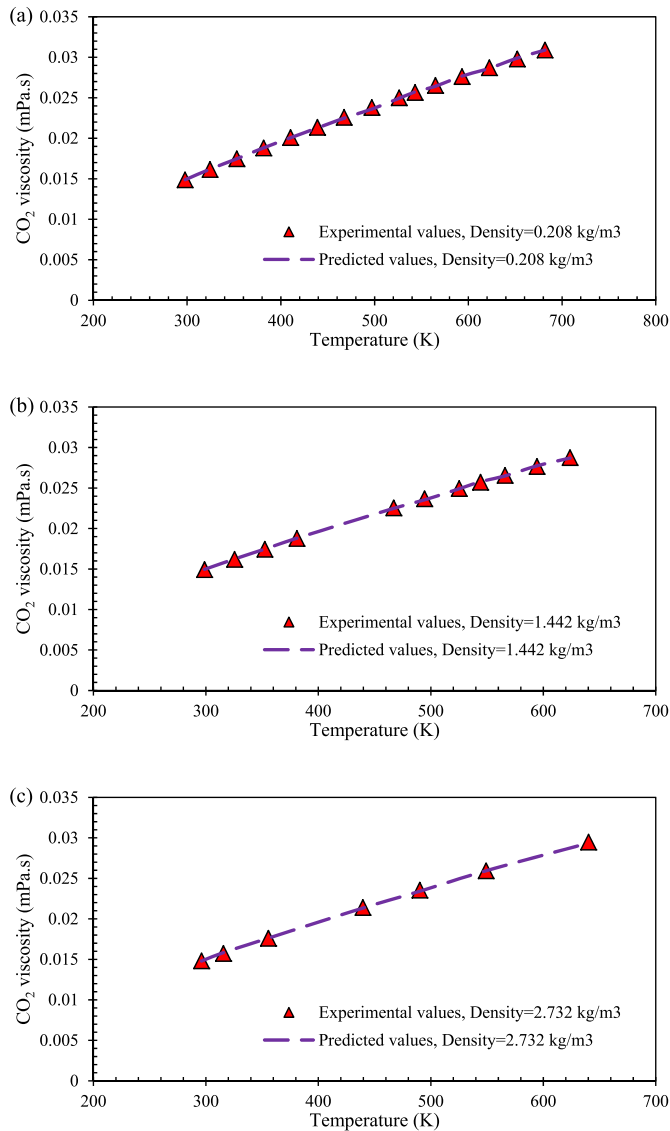
(a)

(b)

(c)

Fig. 8. Variation of CO_2 viscosity with respect to temperature for fixed densities. The predicted values are obtained by the calibrated MLP-LM model.

2017) with an RMSE of 0.016 compared to 0.020. The correlations have notably higher RMSE than the machine learning models, but overall, they all have very high performance.

It is worth noting that the proposed GEP-based explicit correlation can be applied more directly than less transparent intelligent schemes and hence, it can more easily be integrated into different software while studying and simulating tasks related to CO_2 utilization. With some programming, intelligent schemes can however also easily be implemented and applied. Hence, there is no practical limitation to the use of our best-established paradigm in this study, namely the MLP-LM model. For illustration, we have developed an Excel macro to allow its application and utilization. The procedure of using this Excel macro is described in Appendix A.

4.3. Trend analysis and relevancy factor

The impact of the input parameters, namely density and temperature on CO_2 viscosity in the developed MLP-LM model is investigated. The variation of CO_2 viscosity with density for several constant temperatures (313.15, 363.15 and 423.15 K) is reported in Fig. 7 together with experimental points. The stable smooth trends passing through the
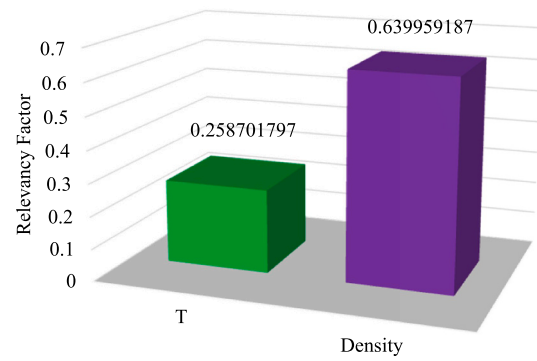

Fig. 9. Relevancy factor.

experimental points indicate the robustness of the newly proposed MLP-LM models in terms of physical interpretation. Fig. 8 also shows CO_2 viscosity versus temperature for constant densities (0.208, 1.442 and 2.732 kg/m^3) with experimental points. The implemented MLP-LM model is able to correctly follow the experimental variations of CO_2 viscosity with temperature.

To quantify the impact of various input parameters on model outputs, the relevancy factor (Pearson correlation coefficient) is normally used. The closer the absolute value of this parameter is to 1, the more the specific input parameter impacts the output (although a linear relation is assumed). The relevancy factor r is defined as follows:

$$r\left(I_j, O\right) = \frac{\sum_{i=1}^{n}\left(I_{j,i} - \overline{I}_j\right)\left(O_i - \overline{O}\right)}{\sqrt{\sum_{i=1}^{n}\left(I_{j,i} - \overline{I}_j\right)^2 \sum_{i=1}^{n}\left(O_i - \overline{O}\right)^2}} \quad (22)$$

where I_j indicates the jth model input (here $j = 2$, and include temperature and density). $I_{j,i}$ is the ith value of input j and $\overline{I}_j$ denotes the average of these values. O_i is the output corresponding to input $I_{j,i}$, and $\overline{O}$ is the average of the output values. As depicted in Fig. 9, the viscosity of CO_2 correlates positively with both input parameters, as given by relevancy factors of 0.26 for temperature and 0.64 for density. Hence, increasing density or temperature is expected to result in rising CO_2 viscosity. Furthermore, as density exhibits higher relevancy factor than temperature, it has more influence on the calculated CO_2 viscosity values.

4.4. Outlier detection

The statistical validity of the developed model in predicting CO_2 viscosity is analyzed using the Leverage statistical approach: the standardized residuals which represent the difference between the forecasted results and the experimental data, and statistical Hat matrix Leverage values are depicted in the Williams plot (standardized
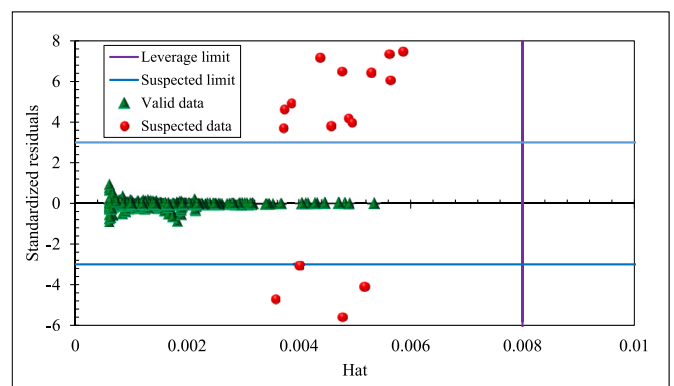

Fig. 10. Williams plot of the best proposed model.

residuals versus Leverage indices) to detect possible outliers. The Hat matrix is calculated using the formula below (Kamari et al., 2015; Jaworska et al., 2005):

$$H = X(X^t X)^{-1} X^t \tag{23}$$

with X represents an (n × d) matrix, n and d denote the dimension and the data points number, respectively, and X^t is the transpose matrix of X. In the Williams plot, a limit Leverage value (H*), which is a constant, has been computed as though $3(d + 1)/n$. The data points are selected in the range of ±3 of standard deviations from the mean, where the cut-off value of 3 covers 99% of the distributed data. To obtain a valid model which leads to predictions in the applicable domain, the majority of data points must be situated in the intervals $0 \leq H \leq H^*$ and $-3 \leq R \leq 3$.

The Williams plot of the MLP-LM model is shown in Fig. 10. The majority of data points are in the ranges of $-3 \leq R \leq 3$ and $0 \leq H \leq 0.008$ and only 1.96% of data points are located outside the applicability domain of the model. It means that most of the data is sufficiently predicted and the validity of the model is confirmed. Therefore, it can be stated that the developed model predicts CO_2 viscosity with high accuracy.

5. Conclusions

In this paper, several machine learning techniques were applied to establish robust and simple-to-use models to accurately predict the viscosity of CO_2 under wide ranges of pressure and temperature conditions, using density and temperature as input parameters. A dataset of 1128 experimental points was used to calibrate and validate the models. Multilayer Perceptron optimized with four distinct back-propagation algorithms, including LM, BR, SCG and RB, and two robust 'white-box' techniques yielding explicit correlations, namely GMDH and GEP, were the applied data-driven methods.

The analysis revealed that MLP optimized with LM (MLP-LM) resulted in the best paradigm for predicting the viscosity of CO_2 with very low RMSE values: 0.0012 during the training, 0.0011 for the test data and 0.0012 as overall value. In addition, the best of the newly proposed models outperformed prior paradigms; The MLP-LM model performed better than the previous best performing intelligent model by Abdolbaghi et al. (2019); also, the best explicit correlation we obtained, from GEP, outperformed the best available explicit correlation, by Laesecke and Muzney (Laesecke and Muzny, 2017). Trend analysis of the MLP-LM model demonstrated that increasing temperature or density causes the viscosity of CO_2 to increase, in line with experimental trends.

Declaration of competing interests

The authors declare that they have no known competing financial interests or personal relationships that could have appeared to influence the work reported in this paper.

CRediT authorship contribution statement

Menad Nait Amar: Writing - original draft. **Mohammed Abdelfetah Ghriga:** Writing - original draft. **Hocine Ouaer:** Writing - original draft. **Mohamed El Amine Ben Seghier:** Writing - original draft, Project administration. **Binh Thai Pham:** Writing - original draft. **Pål Østebø Andersen:** Writing - original draft, Project administration.

Acknowledgments

Appendix A. Supplementary data

References

Abas, N., Khan, N., 2014. Carbon conundrum, climate change, CO2 capture and consumptions. J. CO2 Util 8, 39–48.

Abdolbaghi, S., Barati-Harooni, A., Najafi-Marghmaleki, A., 2019. Improving the prediction ability of reference correlation for viscosity of carbon dioxide. J. CO2 Util 31, 106–114.

Abramson, E.H., 2009. Viscosity of carbon dioxide measured to a pressure of 8 GPa and temperature of 673 K. Phys. Rev. E 80, 21201.

Adams, E.E., Caldeira, K., 2008. Ocean storage of CO2. Elements 4, 319–324.

Ahmadi, M.-A., Ahmadi, M.H., Alavi, M.F., Nazemzadegan, M.R., Ghasempour, R., Shamshirband, S., 2018. Determination of thermal conductivity ratio of CuO/ethylene glycol nanofluid by connectionist approach. J. Taiwan Inst. Chem. Eng. 91, 383–395.

Al-Bayati, D., Saeedi, A., Myers, M., White, C., Xie, Q., Clennell, B., 2018. Insight investigation of miscible SCCO2 Water Alternating Gas (WAG) injection performance in heterogeneous sandstone reservoirs. J. CO2 Util 28, 255–263.

Aminu, M.D., Nabavi, S.A., Rochelle, C.A., Manovic, V., 2017. A review of developments in carbon dioxide storage. Appl. Energy 208, 1389–1419.

Ampelli, C., Perathoner, S., Centi, G., 2015. CO2 utilization: an enabling element to move to a resource-and energy-efficient chemical and fuel production. Philos Trans. R Soc. A Math. Phys. Eng. Sci. 373, 20140177.

Aslam, A., Thomas-Hall, S.R., Manzoor, M., Jabeen, F., Iqbal, M., Uz Zaman, Q., et al., 2018. Mixed microalgae consortia growth under higher concentration of CO2 from unfiltered coal fired flue gas: fatty acid profiling and biodiesel production. J. Photochem. Photobiol. B Biol. 179, 126–133.

Ayegba, P.O., Abdulkadir, M., Hernandez-Perez, V., Lowndes, I.S., Azzopardi, B.J., 2017. Applications of artificial neural network (ANN) method for performance prediction of the effect of a vertical 90° bend on an air–silicone oil flow. J. Taiwan Inst. Chem. Eng. 74, 59–64.

Benamara, C., Nait Amar, M., Gharbi, K., Hamada, B., 2019a. Modeling wax disappearance temperature using advanced intelligent frameworks. Energy Fuels 33, 10959–10968. https://doi.org/10.1021/acs.energyfuels.9b03296.

Benamara, C., Gharbi, K., Nait Amar, M., Hamada, B., 2019b. Prediction of wax appearance temperature using artificial intelligent techniques. Arabian J. Sci. Eng. 1–12. https://doi.org/10.1007/s13369-019-04290-y.

Busch, A., Alles, S., Gensterblum, Y., Prinz, D., Dewhurst, D.N., Raven, M.D., et al., 2008. Carbon dioxide storage potential of shales. Int J Greenh Gas Control 2, 297–308.

Chen, Q., Lv, M., Tang, Z., Wang, H., Wei, W., Sun, Y., 2016. Opportunities of integrated systems with CO2 utilization technologies for green fuel & chemicals production in a carbon-constrained society. J. CO2 Util 14, 1–9.

Chung, T.H., Ajlan, M., Lee, L.L., Starling, K.E., 1988. Generalized multiparameter correlation for nonpolar and polar fluid transport properties. Ind. Eng. Chem. Res. 27, 671–679.

Cole, S., Itani, S., 2013. The alberta carbon trunk line and the benefits of CO2. Energy Procedia 37, 6133–6139.

Cuéllar-Franca, R.M., Azapagic, A., 2015. Carbon capture, storage and utilisation technologies: a critical analysis and comparison of their life cycle environmental impacts. J. CO2 Util 9, 82–102.

Dargahi-Zarandi, A., Hemmati-Sarapardeh, A., Hajirezaie, S., Dabir, B., Atashrouz, S., 2017. Modeling gas/vapor viscosity of hydrocarbon fluids using a hybrid GMDH-type neural network system. J. Mol. Liq. 236, 162–171.

Eshkalak, M.O., Al-shalabi, E.W., Sanaei, A., Aybar, U., Sepehrnoori, K., 2014, November. Enhanced gas recovery by CO2 sequestration versus re-fracturing treatment in unconventional shale gas reservoirs. In: Abu Dhabi International Petroleum Exhibition and Conference. Society of Petroleum Engineers. https://doi.org/10.2118/154329-MS.

Eshraghi, S.E., Rasaei, M.R., Zendehboudi, S., 2016. Optimization of miscible CO2 EOR and storage using heuristic methods combined with capacitance/resistance and Gentil fractional flow models. J. Nat. Gas Sci. Eng. 32, 304–318.

Estrada-Alexanders, A.F., Hurly, J.J., 2008. Kinematic viscosity and speed of sound in gaseous CO, CO2, SiF4, SF6, C4F8, and NH3 from 220 K to 375 K and pressures up to 3.4 MPa. J. Chem. Thermodyn. 40, 193–202.

Fan, T.-B., Wang, L.-S., 2006. A viscosity model based on Peng–Robinson equation of state for light hydrocarbon liquids and gases. Fluid Phase Equil. 247, 59–69.

Fenghour, A., Wakeham, W.A., Vesovic, V., 1998. The viscosity of carbon dioxide. J. Phys. Chem. Ref. Data 27, 31–44.

Ferreira, C., 2001. Algorithm for solving gene expression programming: a new adaptive problems. Complex Syst. 13, 87–129.

Gambhir, A., Napp, T., Hawkes, A., Höglund-Isaksson, L., Winiwarter, W., Purohit, P., et al., 2017. The contribution of non-CO2 greenhouse gas mitigation to achieving long-term temperature goals. Energies 10, 602.

Gerdemann, S.J., O'Connor, W.K., Dahlin, D.C., Penner, L.R., Rush, H., 2007. Ex situ aqueous mineral carbonation. Environ. Sci. Technol. 41, 2587–2593.

Golub'ev, I.F., 1970. Viscosity of Gases and Gas Mixtures: A Handbook. Israel Program for Scientific Translations [available from: the US Department~.

Gong, Y., Gu, Y., 2015. Miscible CO2 simultaneous water-and-gas (CO2-SWAG) injection in the Bakken formation. Energy Fuels 29, 5655–5665.

Guo, X.-Q., Wang, L.-S., Rong, S.-X., Guo, T.-M., 1997. Viscosity model based on equations of state for hydrocarbon liquids and gases. Fluid Phase Equil. 139, 405–421.

Haepp, H.J., 1976. Messung der Viskosität von Kohlendioxid und Propylen. Wärme-Und Stoffübertragung 9, 281–290.

Haykin, S., 2001. Neural Networks and Learning Machines Third Edition, vol. 40. Pearson Upper, Saddle River, NJ, USA. https://doi.org/10.1002/1521-3773 (20010316)40:6<9823::AID-ANIE9823>3.3.CO;2-C.

Hemmati-Sarapardeh, A., Mohagheghian, E., 2017. Modeling interfacial tension and minimum miscibility pressure in paraffin-nitrogen systems: application to gas injection processes. Fuel 205, 80–89.

Hemmati-Sarapardeh, A., Alipour-Yeganeh-Marand, R., Naseri, A., Safiabadi, A., Gharagheizi, F., Ilani-Kashkouli, P., et al., 2013. Asphaltene precipitation due to natural depletion of reservoir: determination using a SARA fraction based intelligent model. Fluid Phase Equil. 354, 177–184.

Hemmati-Sarapardeh, A., Ameli, F., Varamesh, A., Shamshirband, S., Mohammadi, A.H., Dabir, B., 2018a. Toward generalized models for estimating molecular weights and acentric factors of pure chemical compounds. Int. J. Hydrogen Energy 43, 2699–2717.

Hemmati-Sarapardeh, A., Varamesh, A., Husein, M.M., Karan, K., 2018b. On the evaluation of the viscosity of nanofluid systems: modeling and data assessment. Renew. Sustain. Energy Rev. 81, 313–329.

Hendl, S., Neumann, A.-K., Vogel, E., 1993. The viscosity of carbon dioxide and its initial density dependence. High. Temp. - High. Press. 25, 503–511.

Hoffman, B.T., others, 2012, January. Comparison of various gases for enhanced recovery from shale oil reservoirs. In: SPE improved oil recovery symposium. Society of Petroleum Engineers. https://doi.org/10.2118/172083-MS.

Islam, A.W., Carlson, E.S., 2012. Viscosity models and effects of dissolved CO2. Energy Fuels 26, 5330–5336.

Ivakhnenko, A.G., 1971. Polynomial theory of complex systems. IEEE Trans Syst Man Cybern 364–378.

Javadian, H., Asadollahpour, S., Ruiz, M., Sastre, A.M., Ghasemi, M., Asl, S.M.H., et al., 2018. Using fuzzy inference system to predict Pb (II) removal from aqueous solutions by magnetic Fe3O4/H2SO4-activated Myrtus Communis leaves carbon nanocomposite. J. Taiwan Inst. Chem. Eng. 91, 186–199.

Jaworska, J., Nikolova-Jeliazkova, N., Aldenberg, T., 2005. QSAR applicability domain estimation by projection of the training set descriptor space: a review. ATLA-NOTTINGHAM- 33, 445.

Jin, L., Hawthorne, S., Sorensen, J., Pekot, L., Kurz, B., Smith, S., et al., 2017. Advancing CO2 enhanced oil recovery and storage in unconventional oil play—experimental studies on Bakken shales. Appl. Energy 208, 171–183.

Kamari, A., Safiri, A., Mohammadi, A.H., 2015. Compositional model for estimating asphaltene precipitation conditions in live reservoir oil systems. J. Dispersion Sci. Technol. 36, 301–309.

Kestin, J., Whitelaw, J.H., 1963. A relative determination of the viscosity of several gases by the oscillating disk method. Physica 29, 335–356.

Khatiwala, S., Tanhua, T., Mikaloff Fletcher, S., Gerber, M., Doney, S.C., Graven, H.D., et al., 2013. Global ocean storage of anthropogenic carbon. Biogeosciences 10, 2169–2191.

Klewiah, I., Berawala, D.S., Walker, H.C.A., Andersen, Pål, Nadeau, P.H., 2020. Review of experimental sorption studies of CO2 and CH4 in shales. J. Nat. Gas Sci. Eng. 73, 103045.

Koza, J.R., 1992. Genetic Programming II, Automatic Discovery of Reusable Subprograms. MIT Press, Cambridge, MA.

Kumar, P.S., Hogendoorn, J.A., Feron, P.H.M., Versteeg, G.F., 2003. Equilibrium solubility of CO2 in aqueous potassium taurate solutions: Part 1. Crystallization in carbon dioxide loaded aqueous salt solutions of amino acids. Ind. Eng. Chem. Res. 42, 2832–2840.

Laesecke, A., Muzny, C.D., 2017. Reference correlation for the viscosity of carbon dioxide. J. Phys. Chem. Ref. Data 46, 13107.

Li, H., Wilhelmsen, Ø., Lv, Y., Wang, W., Yan, J., 2011. Viscosities, thermal conductivities and diffusion coefficients of CO2 mixtures: review of experimental data and theoretical models. Int J Greenh Gas Control 5, 1119–1139.

Li, P., Chen, J.J.J., Norris, S., 2016. Review of flow condensation of CO2 as a refrigerant. Int. J. Refrig. 72, 53–73.

Liu, Z., Cheng, Y., Wang, Y., Wang, L., Li, W., 2019. Experimental investigation of CO2 injection into coal seam reservoir at in-situ stress conditions for enhanced coalbed methane recovery. Fuel 236, 709–716.

Mazzotti, M., Pini, R., Storti, G., 2009. Enhanced coalbed methane recovery. J. Supercrit. Fluids 47, 619–627.

Michels, A., Botzen, A., Schuurman, W., 1957. The viscosity of carbon dioxide between 0 C and 75 C and at pressures up to 2000 atmospheres. Physica 23, 95–102.

Nait Amar, M., Zeraibi, N., 2019. An efficient methodology for multi-objective optimization of water alternating CO2 EOR process. J. Taiwan Inst. Chem. Eng. 99, 154–165.

Nait Amar, M., Zeraibi, N., Hemmati-Sarapardeh, A., Shamshirband, S., 2019a. Modeling temperature-based oil-water relative permeability by integrating advanced intelligent models with grey wolf optimization: application to thermal enhanced oil recovery processes. Fuel 242, 649–663.

Nait Amar, M., Hemmati-Sarapardeh, A., Varamesh, A., Shamshirband, S., 2019b. Predicting solubility of CO2 in brine by advanced machine learning systems: application to carbon capture and sequestration. J. CO2 Util 33, 83–95.

Norhasyima, R.S., Mahlia, T.M.I., 2018. Advances in CO₂ utilization technology: a patent landscape review. J. CO2 Util 26, 323–335.

Nuttal, B.C., 2010. Reassessment of CO 2 Sequestration Capacity and Enhanced Gas Recovery Potential of Middle and Upper Devonian Black Shales in the Appalachian Basin. MRCSP Phase II Topical Report October 2005–October 2010. Midwest Regional Carbon Sequestration Partnership.

Oelkers, E.H., Gislason, S.R., Matter, J., 2008. Mineral carbonation of CO2. Elements 4, 333–337.

Ouaer, H., Hosseini, A.H., Amar, M.N., Seghier, M., Ghriga, M.A., Nabipour, N., et al., 2020. Rigorous connectionist models to predict carbon dioxide solubility in various ionic liquids. Appl. Sci. 10, 304.

Pu, W., Wei, B., Jin, F., Li, Y., Jia, H., Liu, P., et al., 2016. Experimental investigation of CO2 huff-n-puff process for enhancing oil recovery in tight reservoirs. Chem. Eng. Res. Des. 111, 269–276.

Raja, M.A.Z., Ahmed, T., Shah, S.M., 2017. Intelligent computing strategy to analyze the dynamics of convective heat transfer in MHD slip flow over stretching surface involving carbon nanotubes. J. Taiwan Inst. Chem. Eng. 80, 935–953.

Rostami, A., Hemmati-Sarapardeh, A., Karkevandi-Talkhooncheh, A., Husein, M.M., Shamshirband, S., Rabczuk, T., 2019. Modeling heat capacity of ionic liquids using group method of data handling: a hybrid and structure-based approach. Int. J. Heat Mass Tran. 129, 7–17.

Sawalha, S., Piscopiello, S., Karampour, M., Manickam, L., Rogstam, J., 2017. Field measurements of supermarket refrigeration systems. Part II: analysis of HFC refrigeration systems and comparison to CO2 trans-critical. Appl. Therm. Eng. 111, 170–182.

Schäfer, M., Richter, M., Span, R., 2015. Measurements of the viscosity of carbon dioxide at temperatures from (253.15 to 473.15) K with pressures up to 1.2 MPa. J. Chem. Thermodyn. 89, 7–15.

Sheng, J.J., 2015. Enhanced oil recovery in shale reservoirs by gas injection. J. Nat. Gas Sci. Eng. 22, 252–259.

Shokir, E.M.E.-M., Hamed, M.M.B., Ibrahim, A.E.-S., Mahgoub, I., 2017. Gas lift optimization using artificial neural network and integrated production modeling. Energy Fuels 31, 9302–9307.

Span, R., Wagner, W., 1996. A new equation of state for carbon dioxide covering the fluid region from the triple-point temperature to 1100 K at pressures up to 800 MPa. J. Phys. Chem. Ref. Data 25, 1509–1596.

Taher, H., Al-Zuhair, S., Al-Marzouqi, A., Haik, Y., Farid, M., 2015. Growth of microalgae using CO2 enriched air for biodiesel production in supercritical CO2. Renew. Energy 82, 61–70.

Teodorescu, L., Sherwood, D., 2008. High energy physics event selection with gene expression programming. Comput. Phys. Commun. 178, 409–419.

Van Der Gulik, P.S., 1997. Viscosity of carbon dioxide in the liquid phase. Phys. A Stat. Mech. Its Appl. 238, 81–112.

Venkatraman, V., Alsberg, B.K., 2017. Predicting CO2 capture of ionic liquids using machine learning. J. CO2 Util 21, 162–168.

Vesovic, V., Wakeham, W.A., Olchowy, G.A., Sengers, J.V., Watson, J.T.R., Millat, J., 1990. The transport properties of carbon dioxide. J. Phys. Chem. Ref. Data 19, 763–808.

Vogel, E., 2016. The viscosities of dilute Kr, Xe, and CO $$ _ $$ revisited: new experimental reference data at temperatures from 95 K to 690 K. Int. J. Thermophys. 37, 63.

Vogel, E., Barkow, L., 1986. Precision measurements of the viscosity coefficient of carbon dioxide between room temperature and 650 K. Z. Phys. Chem. 267, 1038–1043.

Yu, W., Lashgari, H., Sepehrnoori, K., others, 2014. Simulation study of CO2 huff-n-puff process in Bakken tight oil reservoirs. In: SPE West. North Am. Rocky Mt. Jt. Meet..

Yu, W., Lashgari, H.R., Wu, K., Sepehrnoori, K., 2015. CO2 injection for enhanced oil recovery in Bakken tight oil reservoirs. Fuel 159, 354–363.

Zhang, Z.X., Wang, G.X., Massarotto, P., Rudolph, V., 2006. Optimization of pipeline transport for CO2 sequestration. Energy Convers. Manag. 47, 702–715.

Zhang, Z., Li, H., Chang, H., Pan, Z., Luo, X., 2018. Machine learning predictive framework for CO 2 thermodynamic properties in solution. J. CO2 Util 26, 152–159.